Liquid Crystals
Publication details, including instructions for authors and subscription information:
http://www.informaworld.com/smpp/title~content=t713926090

Pyridinium salt liquid crystals Effect of mesogen extension and alkyl chain length

Maryam Tabrizian[ab]; Armand Soldera[a]; Michel Couturier[a]; C. Geraldine Bazuin[a]
[a] Centre de recherche en sciences et ingénierie des macromolécules (CERSIM), Département de chimie, Université Laval, Québec, Canada [b] INRS-Énergie et Matériaux, 1650 montée Sainte-Julie, Québec, Canada

To cite this Article Tabrizian, Maryam , Soldera, Armand , Couturier, Michel and Bazuin, C. Geraldine(1995) 'Pyridinium salt liquid crystals Effect of mesogen extension and alkyl chain length', Liquid Crystals, 18: 3, 475 — 482
To link to this Article: DOI: 10.1080/02678299508036647
URL: http://dx.doi.org/10.1080/02678299508036647

LIQUID CRYSTALS, 1995, VOL. 18, NO. 3, 475–482

Pyridinium salt liquid crystals
Effect of mesogen extension and alkyl chain length

by MARYAM TABRIZIAN†, ARMAND SOLDERA, MICHEL COUTURIER
and C. GERALDINE BAZUIN*

Centre de recherche en sciences et ingénierie des macromolécules (CERSIM), Département de chimie, Université Laval, Québec, G1K 7P4, Canada

(*Received 6 April 1994; accepted 10 June 1994*)

The thermotropism of 1-*n*-alkyl-(4-methyl and 4-tolyl)pyridinium bromides were compared for alkyl chain lengths ranging from $n = 12$ to 22 carbons. A smectic A mesophase is present in both series for the longer chain compounds, $n \geq 16$, with the clearing temperature being similar for both series but increasing rapidly with chain length. The series with the elongated mesogen also possesses an ordered mesophase identified as smectic G. The transition between this mesophase and the S_A or isotropic phase in the 4-tolyl series, and the transition to and from the crystalline phase in both series, are affected relatively little by the alkyl chain length. It seems that the S_A mesophase is governed primarily by the amphiphilic character of the substances, whereas elongation of the ionic head group is responsible for the appearance of a more ordered mesophase at intermediate temperatures.

1. Introduction

The vast majority of thermotropic liquid crystals that have been studied are based on elongated aromatic mesogens [1]. Fewer studies have been devoted to the thermotropism of liquid crystals with ionic head groups. Of these, attention has been focused in particular on various metal alkanoates [1, 2], and, to a lesser extent, on alkyl ammonium salts [1, 3], generally without aromatic groups involved.

A small number of investigations have been made of ionic liquid crystals in which the ionic head group is at the same time aromatic, albeit with only a single ring, notably pyridinium salts [4–6]. They are considered to be intermediate between what are classically distinguished as mesogenic (aromatic core) and amphiphilic (ionic core) liquid crystals. In this paper, we report on the effect of increasing the length of the aromatic core on the liquid crystalline character of these materials, as a function of alkyl chain length. For this purpose, two series of *n*-alkyl pyridinium bromide derivatives, shown in figure 1, were synthesized.

2. Experimental

2.1. *Apparatus*

Investigation of the liquid crystalline polymorphism was carried out using differential scanning calorimetry (DSC), polarized optical microscopy and X-ray diffraction. DSC measurements were conducted with a Perkin–Elmer DSC-4 apparatus calibrated with pure indium. Melting (crystallization) curves were recorded at a heating (cooling) rate of $2{\cdot}5°C\,min^{-1}$; the melting (crystallization) temperatures reported are the onset temperatures. The transition temperatures were verified, and the microscopic textures observed, with a Zeiss Axioskop polarizing optical microscope equipped with a Mettler FP52/FP5 controlled hot stage and a Leica objective. X-ray diffraction patterns of powdered samples, packed in Lindemann capillaries, were recorded by a scintillation counter coupled with a pulse-height analyser as detector using Ni-filtered CuK_α radiation ($\lambda = 1{\cdot}542$ Å) from a Rigaku rotating anode generator (Rotaflex RU200). Collimation was effected at wide angles with a Soller slit and a 1·0 mm pinhole. Temperature was controlled by a water-cooled copper block oven with Mylar windows.

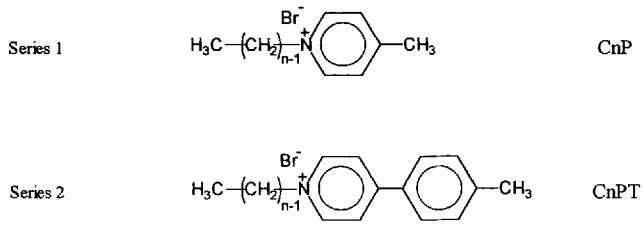

Figure 1. Schematic representation of the compounds composing series 1 (C*n*P) and 2 (C*n*PT); $n = 12$, 16, 22.

* Author for correspondence.
† Present address: INRS-Énergie et Matériaux, 1650 montée Sainte-Julie, Varennes, Québec, J3X 1S2, Canada.

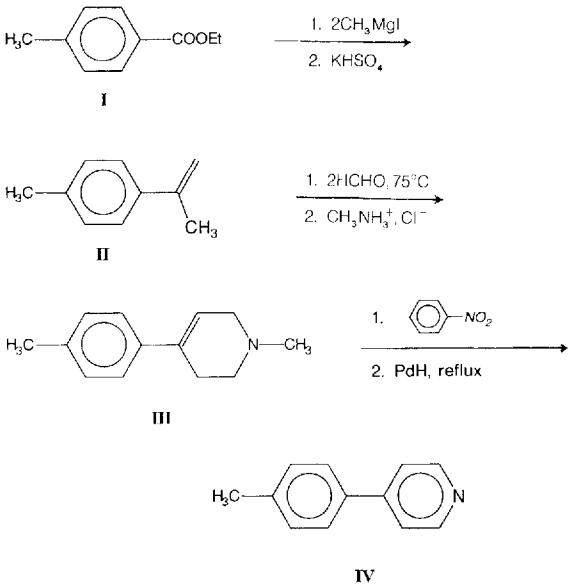

Figure 2. Schematic synthesis route for the preparation of the mesogenic head group of series 2.

2.2. *Synthesis*

2.2.1. *Preparation of the mesogenic core of series 2*

The synthetic scheme, based on [7] and [8] is shown in figure 2; it involves three main steps. The first is the synthesis of 4-methyl cumene (**II**) from ethyl-4-methylbenzoate (**I**) (Aldrich). Thus, 16·4 g (0·1 mol) of **I**, used as is, were added slowly to a solution of 100 ml (0·3 mol) of methyl magnesium bromide in anhydrous diethyl ether, under nitrogen, followed by 12 h of stirring at ambient temperature. The solution, containing 4-isopropanol toluene, was then treated with a catalytic quantity of $KHSO_4$ at 95–100°C for 1 h. The desired product, **II**, a colourless oil, was isolated by distillation under reduced pressure. Yield 76 per cent; b.p. 122°C/88 mm Hg. ^{1}H NMR (Bruker 200 MHz, $CDCl_3$): $\delta = 2{\cdot}20$ (3 H, s, CH_3 aliphatic), 2·41 (3 H, s, CH_3 aromatic), 5·10 (1 H, m, allylic), 5·40 (1 H, s, allylic), 7·18–7·22 (2 H, d, aromatic), 7·41–7·45 (2 H, d, aromatic).

In the second step, 13·2 g (0·1 mol) of **II** were dissolved in 100 ml H_2O, to which 13·1 g (0·2 mol) of methyl ammonium chloride were added. With the solution cooled to 0°C, 12 ml (0·2 mol) of formaldehyde (37 per cent in H_2O) were then added, followed by heating at 90°C for 1 h. Subsequently, 10 ml of concentrated H_2SO_4 were added dropwise. After completion of the reaction, the solution was cooled, poured into 500 ml of basic water, and the desired product, 1-methyl-4-tolyl-2,3,6-hydropyridine (**III**), was extracted with benzene. The organic phase was dried over $MgSO_4$ and concentrated. The product was then distilled and washed with cold petroleum ether, yielding a white powder. Yield 56 per cent, b.p. 120°C/1·5 mm Hg. ^{1}H NMR (200 MHz, $CDCl_3$): $\delta = 2{\cdot}33$ (3 H, s, CH_3N), 2·40 (3 H, s, CH_3 aromatic), 2·55–2·7 (4 H, m, 5,6-hydropyridine), 3·10 (2 H, m, 3-hydropyridine), 6·01 (1 H, m, 2-hydropyridine), 7·10–7·14 (2 H, d, aromatic), 7·26–7·30 (2 H, d, aromatic).

For the last step, 9 g (0·05 mol) of **III** were added to 200 ml of a heterogeneous solution of diethyl ether and water containing 7 g (0·1 mol) of nitrobenzene. A catalytic quantity of PdH was then added. The mixture was stirred at reflux for 1 h, then poured into diethyl ether. The organic phase was washed consecutively with dilute HCl, dilute NaOH and water, and then dried over $MgSO_4$. The solvent was evaporated, and the product, 4-tolyl-pyridine (**IV**), recrystallized in 40/60 (v/v) ethyl acetate/hexane, yielding white crystals. Yield 65 per cent, m.p. 99°C. ^{1}H NMR (200 MHz, $CDCl_3$): $\delta = 2{\cdot}40$ (3 H, s, CH_3 aromatic), 7·26–7·30 (2 H, d, aromatic), 7·48–7·51 (2 H, m, pyridine), 7·54–7·58 (2 H, d, aromatic), 8·61–8·65 (2 H, m, pyridine).

2.2.2. *Synthesis of the 1-*n*-alkyl-(4-methyl and 4-tolyl)pyridinium bromide compounds*

Grafting of alkyl chains of various lengths to the mesogenic core, either 4-methylpyridine (Aldrich) or 4-tolylpyridine (**IV**), was accomplished via classic quaternization techniques, using appropriate *n*-alkyl bromides (Aldrich), all used as received. The two reagents were reacted in an appropriate solvent under reflux for 12 h; the solution was then cooled and poured into hexane. The resulting precipitate was filtered and precipitated twice more from an appropriate solvent. The final compounds are listed in table 1, with their assigned acronym, yield, the solvent used for the quaternization reaction, and the precipitating solvent. The acronyms, C*n*P and C*n*PT, denote the compounds of series 1 and 2, respectively, with *n* indicating the number of carbons in the alkyl chain. Elemental analysis results (Guelph Chemicals, Ontario) for all the compounds are listed in table 2.

Representative NMR assignments are given for one example each of the series C*n*P and C*n*PT.

1-n-*Hexadecyl-4-methylpyridinium bromide* (*C16P*). ^{1}H NMR (200 MHz, $CDCl_3$): $\delta = 0{\cdot}82$–$0{\cdot}88$ (3 H, t, CH_3 aliphatic), 1·2–1·4 (26 H, m, aliphatic), 2·0 (2 H, m, $C\underline{H}_2CH_2N^+$), 2·65 (3 H, s, CH_3 aromatic), 4·87–4·94 (2 H, t, CH_2N^+) 7·85–7·88 (2 H, d, 2CHCHN$^+$), 9·28–9·31 (2 H, d, 2CHN$^+$).

1-n-*Hexadecyl-4-tolylpyridinium bromide* (*C16PT*). ^{1}H NMR (200 MHz, $CDCl_3$): $\delta = 0{\cdot}85$ (3 H, t, CH_3 aliphatic), 1·2–1·4 (26 H, m, aliphatic), 2·0–2·1 (2 H, m, $C\underline{H}_2CH_2N^+$), 2·45 (3 H, s, CH_3 aromatic), 4·89–4·96 (2 H, t, CH_2N^+), 7·35–7·39 (2 H, d, aromatic), 7·68–7·72

Table 1. Acronyms, number of carbon atoms in the alkyl chain (n), solvent used for the quaternization reaction, yield, and precipitating solvent for each product synthesized.

Acronym	n	Solvent	Yield/per cent	Precipitant
C12P	12	4-Picoline	76	Hexane
C16P	16	4-Picoline	65	Ether
C22P	22	4-Picoline/2-Propanol	54	Ether
C12PT	12	Acetonitrile	75	Hexane/ether
C16PT	16	Acetonitrile/2-Propanol	55	Hexane/ether
C22PT	22	2-Propanol	46	Ether

(2 H, d, aromatic), 8·19–8 22 (2 H, d, 2CHCHN$^+$), 9·40–9·43 (2 H, d, 2CHN$^+$).

In addition, a singlet due to bound H_2O at $\delta = 1{\cdot}7$–$1{\cdot}8$ frequently appeared in the spectra of the dried compounds, generally corresponding to half a water molecule or less per pyridinium–bromide ion pair. This agrees with what was noted by Navarro-Rodriguez *et al.* [9], for ω-substituted N-alkylpyridinium bromides. The bound water is relatively difficult to remove, and can also be observed in some of the elemental analysis results (see table 2). Just prior to investigation, the powdered samples were routinely dried at 80°C under reduced pressure overnight. Based on the NMR spectra obtained after this treatment, we conclude that there is at most half a water molecule per ion pair in the samples studied.

3. Results

The mesophase structures, transition temperatures and corresponding enthalpies of the two series of compounds studied, along with the Bragg spacings, d, from small angle X-ray diffraction data and calculated molecular lengths, l, for the disordered mesophase of each compound, are collected in tables 3 and 4. The meaning of these data, with explanatory details, are given in the next two sections, treating the two series separately.

3.1. *Series 1*

The two longest chain compounds of the 4-methyl-1-n-alkylpyridinium bromides, C22P and C16P, show two transitions, the lower temperature one with a large enthalpy typical of order–disorder transitions, and the higher temperature one with a small enthalpy characteristic of transitions involving disordered liquid crystals. Both transitions are reversible, with significant supercooling for the lower temperature transition; the onset of the higher temperature transition is similar in heating and in cooling. For C22P, the sample undergoes degradation above the highest temperature transition at

Table 2. Elemental analysis results.

Sample	Empirical formula		C/per cent	H/per cent	Br/per cent
C12P	$C_{18}H_{32}NBr$	Calculated	63·14	9·42	23·34
		Measured	63·27	9·68	23·05
C16P	$C_{22}H_{40}NBr$	Calculated	66·31	10·20	20·05
		Measured	65·97	10·38	20·32
C22P	$C_{28}H_{52}NBr$	Calculated	69·68	10·86	16·56
	$C_{28}H_{52}NBr \cdot H_2O$	Calculated	67·17	10·87	15·96
		Measured	66·92	11·11	15·95
C12PT		Calculated	68·88	8·67	19·10
	$C_{24}H_{36}NBr$	Calculated	66·04	8·76	18·31
	$C_{24}H_{36}NBr \cdot H_2O$	Measured	65·45	8·80	18·38
C16PT	$C_{28}H_{44}NBr$	Calculated	70·86	9·35	16·84
	$C_{28}H_{44}NBr \cdot H_2O$	Calculated	68·27	9·41	16·22
		Measured	68·02	9·55	16·47
C22PT	$C_{34}H_{56}NBr$	Calculated	73·09	10·10	14·30
		Measured	72·80	10·23	14·41

Table 3. Series 1: transition temperatures at onset (T) and enthalpies (ΔH) from DSC, experimental layer spacings (d_{S_A}) determined from small angle X-ray diffraction, and calculated lengths (l) of the molecules in their most extended conformation; the Ts and ΔHs determined on cooling are given in italics.

Sample	C	T/°C	ΔH/kJ mol^{-1}	S_A	T/°C	ΔH/kJ mol^{-1}	I	d_{S_A}/Å	l/Å
C12P	●	68	27				●	—	—
	●	*46–41*	*−31*				●		
C16P	●	84	44	●	109	0·3	●	33	33
	●	*65–55*	*−40*	●	*106*	*−0·4*	●		
C18P†	●	92	59	●	158	0·7	●	35	35
	●			●			●		
C22P	●	94	69	●	206	2	●	40	40
	●	*67*	*−34*	●	nd	nd	●		

†[5] (peak temperature).
nd: not determined.

206°C, making it impossible to obtain reliable quantitative data for that transition from DSC cooling curves; however, its reversibility was ascertained from polarizing optical microscopy observations.

The higher temperature mesophase of C16P and C22P, in the polarizing optical microscope, shows the focal-conic texture (bluish in colour) with homeotropic regions characteristic of a smectic A mesophase. In fact, the tendency to form the homeotropic texture was very strong, even when heating from the lower temperature phase. The smectic A assignment was confirmed by X-ray diffraction data showing a diffuse band at wide angles and a sharp band accompanied by a second order diffraction at small angles. The wide angle band was centred at $2\theta = 20°$, which corresponds to a Bragg distance of 4·4 Å, representing the average lateral spacing between disordered alkyl chains. The primary band at small angles corresponds to a Bragg distance identical to that of the molecular length in its most extended conformation (see table 3), thus indicating that the molecules are, on average, perpendicular to the lamellar planes. The lower temperature mesophase has been shown to be crystalline in nature by virtue of the existence of several sharp peaks at both wide and small angles.

These data, and the phase assignments, are altogether consistent with that previously obtained for the compound C18P [5]. The model proposed for that compound in the smectic A mesophase is one where the molecules within a layer are oriented perpendicularly on average to the layer plane in alternate head/tail fashion. An anion lies at the end of each molecule in such a way that it is sandwiched between pyridinium rings of neighbouring molecules. This arrangement results in interdigitation of the anion–pyridinium head groups of neighbouring layers, probably accompanied by some interpenetration of the alkyl chains of the neighbouring layers.

For the compound, C12P, no S_A mesophase is observed; rather, it crystallizes directly from the isotropic liquid as a series of overlapping peaks in DSC beginning from 46°C. On heating from room temperature, there is a small transition, probably a crystal–crystal transition, at 44°C. The melting transition occurs at 68°C with a large enthalpy.

The dependence of the transition temperatures of the CnP series on alkyl chain length is summarized in figure 3 (*a*). Of particular noteworthiness is the very strong dependence of the S_A–isotropic transition temperature on the alkyl chain length, ranging from 206°C for C22P to 158°C for C18P [5] to 109°C for C16P. The transition temperature of the crystalline phase to the disordered or

Table 4. Series 2: transition temperatures at onset (T) and enthalpies (ΔH) from DSC, experimental layer spacings (d_{S_A}) determined from small angle X-ray diffraction, and calculated lengths (l) of the molecules in their most extended conformation; the Ts and ΔHs determined on cooling are given in italics.

Sample	C	T/°C	ΔH/kJ mol^{-1}	S_G	T/°C	ΔH/kJ mol^{-1}	S_A	T/°C	ΔH/kJ mol^{-1}	I	d_{S_A}/Å	l/Å
C12PT	●	95	nd	●	125	nd				●	—	—
	●	*<70*	nd	●	*122*	nd				●		
C16PT	●	80	30	●	152	8				●	—	37
	●	*<60*	nd	●	*151*	*−7*	●	*151·3*	nd	●		
C22PT	●	92	53	●	150	3	●	200	0.5	●	41	45
	●	nd	nd	●	*148*	*−3*	●	nd	nd	●		

nd: not determined.

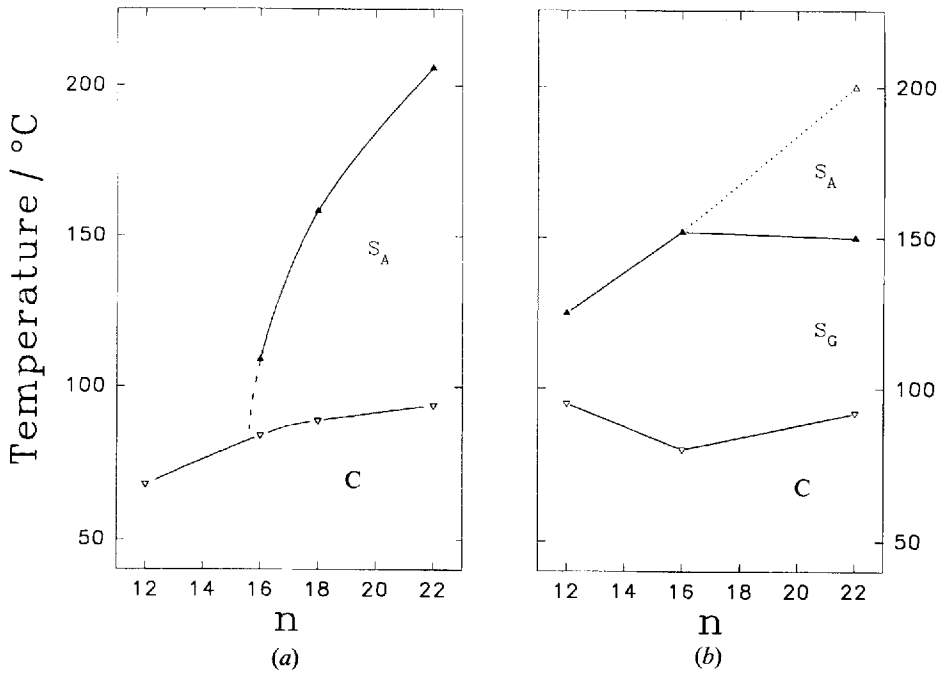

Figure 3. Transition temperatures (onsets), obtained from DSC heating thermograms, as a function of alkyl chain length for (*a*) series 1 (C*n*P) and (*b*) series 2 (C*n*PT); the data for C18P were obtained from [5].

isotropic phase is much less dependent on alkyl chain length than that of the S_A to isotropic phase. These observations were also made by Nusselder *et al.* [6], for 1-methyl-4-*n*-alkylpyridinium iodides and by Knight and Shaw [10] for 1-alkylpyridinium bromides, with chain lengths varying from 12 to 18 carbons.

3.2. *Series 2*

The longest chain compound of this series, C22PT, shows three transition temperatures on heating. Above the highest transition, at 200°C, the compound begins to degrade, thus precluding quantitative DSC cooling data of that transition. The large enthalpy of the lowest temperature transition, succeeded by two transitions with much smaller enthalpies, suggests a crystalline phase at ambient temperature followed by two mesophases on heating.

In the polarizing optical microscope, the transition from the ambient temperature phase to the intermediate mesophase is not obvious; however, the sample is viscous and can be easily sheared in the temperature range of the intermediate mesophase. In heating to the higher temperature mesophase, the sample is very liquid with reduced birefringence, although much more birefringent than for C22P and yellow rather than blue in colour; some homeotropic texture also appears at the higher temperatures. In varying the temperature in this mesophase when above about 170–180°C, there is significant movement, including the transitory appearance of bâtonnets.

Table 5. Bragg spacing of the S_A mesophase of C22PT at various temperatures.

T/°C	d_{001}/Å
150	41·1
130	41·6
105	44·2
95	44·7
85	C

The X-ray diffraction pattern of the highest temperature mesophase shows a diffuse band at wide angles centred at $2\theta = 20°$ and first and second order diffraction bands at small angles, corresponding to a Bragg spacing of 41 Å. This spacing is about 10 per cent smaller than the molecular length of C22PT in its most extended conformation with the bromide anion at its end (see table 4). Given the partially homeotropic texture of this mesophase and the fact that the lamellar spacing increases with decreasing temperature (see below, table 5), which is opposite to what is observed for S_C, this mesophase can be identified as S_A. The same model mentioned above, proposed in [5] is applicable to this mesophase. The lower temperature mesophase is characterized by a more complex diffraction pattern at wide angles, as shown in figure 4(*a*), indicative of an ordered mesophase. First

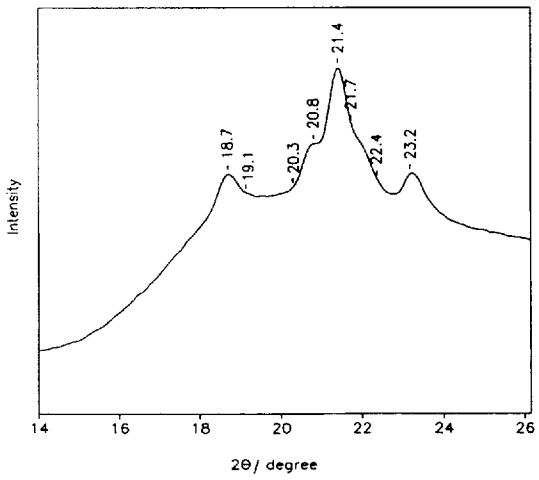

(*a*)

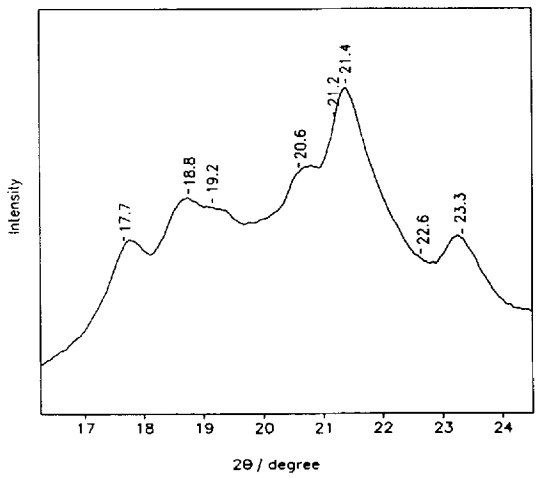

(*b*)

Figure 4. Wide angle X-ray diffraction profiles of (*a*) C22PT and (*b*) C16PT, with the calculated angles corresponding to a monoclinic lattice fit indicated (see text and tables 6 and 7).

and weak second order diffraction peaks at small angles denote a Bragg spacing of 36 Å, which is significantly smaller than one molecular length. Thus, this must be a tilted phase. This topic will be revisited below.

The C16PT compound also presents an S_A and an ordered mesophase; however, the S_A mesophase exists in a very short temperature interval of about 0·5°C. Its presence is detected by the appearance of bâtonnets, in the polarizing optical microscope, upon cooling at faster rates from the isotropic phase. This texture is quickly transformed into a mosaic-type texture via dendritic growth of elongated platelets and splinters, a texture which is also obtained directly by slow cooling from the isotropic phase. The existence of the S_A phase is confirmed by the DSC cooling endotherm (see figure 5), where a distinct shoulder is visible on the high temperature side of the transition at 151°C. The ordered mesophase gives rise to an X-ray diffraction pattern similar to that for C22PT, as shown in figure 4(*b*). Cooling the C12PT compound from the isotropic state results in the direct appearance of the ordered mesophase, as observed under crossed polarizers.

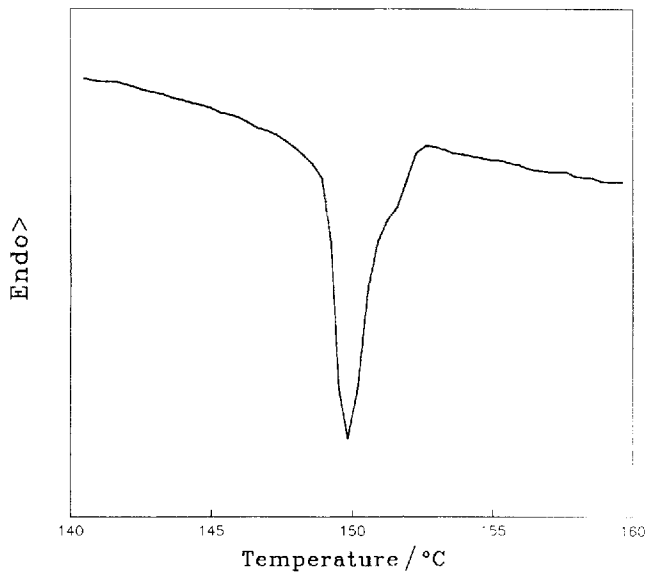

Figure 5. Cooling thermogram at 2·5°C min^{-1} for C16PT.

The viscosity and texture of the ordered mesophase and its X-ray diffraction pattern (see figure 4) appear to be consistent with a smectic G assignment [11]. Hence, the X-ray data were indexed supposing such a structure, that is a C-centred monoclinic unit cell [12–14]. The parameter c, or molecular length, used for the indexing was determined from X-ray analysis of the d_{001} reflection of C22PT at various temperatures, given in table 5. Probably due to the presence of a small amount of degradation resulting from exposure at higher temperatures, the S_A mesophase was maintained to lower temperatures than usual. In decreasing the temperature, the lamellar thickness increases due to decreasing thermal mobility of the alkyl chains. At the lowest temperature measured before crystallization, d_{001} corresponds closely to the calculated molecular length. Given this agreement, it is this value which was used as the parameter c, and which permitted determination of the angle β, knowing the d_{001} reflection of the S_G phase. This procedure is comparable to that used in [15], where the molecular length taken to calculate the angle β for a S_C is that corresponding to the d_{001} reflection at the S_A–S_C transition. The parameter c used for C16PT was determined by subtracting the length of three ethylene groups in *trans*-conformation ($3 \times 2{\cdot}54$ Å) from the c used for C22PT. Thus, with c and β fixed, the parameters a and b were

Table 6. Monoclinic lattice parameters calculated for C22PT at 120°C ($a=10{\cdot}24$, $b=4{\cdot}80$ and $c=44{\cdot}6$ Å, $\beta=127°$).

h	k	l	d_{hkl}/Å	2θ/°
0	0	2	17·88	4·94
0	1	1	4·75	18·67
$\bar{2}$	0	2	4·65	19·08
$\bar{2}$	0	1	4·38	20·26
$\bar{1}$	1	1	4·26	20·84
1	1	0	4·14	21·46
2	0	0	4·10	21·66
1	1	1	3·98	22·35
2	0	1	3·83	23·25

varied to give optimal correspondence between the experimental and calculated values for C22PT and C16PT.

The results are tabulated in tables 6 and 7, and compared with the experimental data in figure 4. Although the scattering maxima are not very well resolved, the calculated angles indicated in figure 4 fit the observable experimental peak positions satisfactorily (there is, however, an unexpected difference between the a values of the two compounds); this suggests that this mesophase is indeed S_G. The C12PT mesophase could not be analysed in the same way for lack of remaining sample.

The transition temperatures as a function of alkyl chain length for the CnPT series are summarized in figure 3 (*b*). The transition from the highest temperature mesophase into the isotropic phase is again rather strongly dependent on the chain length in the range studied, whereas the lower temperature transitions are less sensitive to this factor.

4. Remarks and conclusions

The strong dependence of the S_A–isotropic transition temperature on alkyl chain length for both series of compounds complements the suggestion in [6] that this behaviour may be characteristic of n-alkylpyridinium halides. The increase in clearing temperature with alkyl chain length implies that the amphiphilic character in the compounds, that is the repulsion between the ionic and non-ionic portions, is favoured at long chain lengths, with the maximum at $n \geq 22$ for both series. It is further noteworthy that the S_A–isotropic transition occurs at similar temperatures for C22P and C22PT. This indicates that there is little effect of the elongation of the ionic headgroup on this transition, and suggests that it is the ionic forces that are primarily responsible for maintaining the layer structure of the long chain compounds to high temperatures.

On the other hand, the elongation of the ionic head group is responsible for the appearance of the more ordered S_G mesophase, and thus a richer polymorphism in the CnPT series. The ordered mesophase impinges mainly on the temperature domain of the S_A mesophase, as found in CnP, thus limiting the appearance of the disordered mesophase to higher temperatures. Evidently, the van der Waals repulsive forces between the aromatic and aliphatic portions, typically present in thermotropic mesogens, are now exerting themselves. Somehow, the combination of amphiphilic and van der Waals repulsions in CnPT leads to an inclined mesophase. Perhaps a variation on McMillan's theory relating the formation of smectic C to the presence of outboard dipoles [16] is applicable here. According to the model of [5], considered to represent the S_A mesophase of C22PT, the bromine ions are located both between and at the end of the pyridinium rings. As shown in figure 6, this actually creates lateral dipoles on the aromatic moiety which may be responsible for the inclination of the more ordered mesophase. Alternatively, a preferred (face-to-face) orientation of the pyridinium rings relative to the neighbouring anions, may give rise to steric factors that induce inclination of the molecules, analogous to Wulf's theory for the S_C phase [17].

Table 7. Monoclinic lattice parameters calculated for C16PT at 105°C ($a=11{\cdot}02$, $b=4{\cdot}79$ and $c=36{\cdot}97$ Å, $\beta=130°$).

h	k	l	d_{hkl}/Å	2θ/°
0	0	2	14·1	6·27
$\bar{2}$	0	2	5·01	17·71
0	1	1	4·72	18·81
$\bar{2}$	0	1	4·61	19·24
$\bar{1}$	1	1	4·32	20·57
2	0	0	4·20	21·15
1	1	0	4·16	21·37
1	1	1	3·94	22·59
2	0	1	3·81	23·34

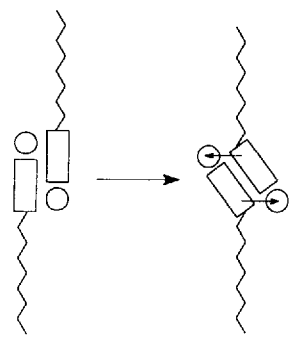

Figure 6. Schematic representation of the passage from an orthogonal to an inclined mesophase for series 2.

Financial support of the research by the Natural Sciences and Engineering Research Council of Canada and by the Fonds pour la Formation de Chercheurs et l'Aide à la Recherche is gratefully acknowledged.

References

[1] KELKER, H., and HATZ, R., 1980, *Handbook of Liquid Crystals* (Verlag Chemie).
[2] GRAY, G. W., and WINSOR, P. A., (editors), 1974, *Liquid Crystals and Plastic Crystals*, Vols. 1 and 2 (Wiley).
[3] NEEDHAM, G. F., WILLETT, R. D., and FRANZEN, H. F., 1984, *J. phys. Chem.*, **88,** 674. GAULT, J. D., GALLARDO, H. A., and MÜLLER, H. J., 1985, *Molec. Crystals liq. Crystals*, **130,** 163. MALLIARIS, A., PALEOS, C. M., and DAIS, P., 1987, *J. phys. Chem.*, **91,** 1149. PALEOS, C. M., TSIOURVAS, D., and DAIS, P., 1989, *Liq. Crystals*, **5,** 1747, and references therein.
[4] SUDHÖLTER, E. J. R., ENGBERTS, J. B. F. N., and DE JEU, W. H., 1982, *J. phys. Chem.*, **86,** 1908.
[5] BAZUIN, C. G., GUILLON, D., SKOULIOS, A., and NICOUD, J.-F., 1986, *Liq. Crystals*, **2,** 181.
[6] NUSSELDER, J. J. H., ENGBERTS, J. B. F. N., and VAN DOREN, H. A., 1993, *Liq. Crystals*, **13,** 213, and references therein.
[7] PERKIN, W. H., and PICKLES, S. S., 1905, *J. chem. Soc.*, **87,** 639.
[8] SCHMIDLE, C. J., LOCKE, J. E., and MANSFIELD, R. C., 1956, *J. org. Chem.*, **21,** 1194.
[9] NAVARRO-RODRIGUEZ, D., FRÈRE, Y., GRAMAIN, P., GUILLON, D., and SKOULIOS, A., 1991, *Liq. Crystals*, **9,** 321.
[10] KNIGHT, G. A., and SHAW, B. D., 1938, *J. chem. Soc.*, p. 682.
[11] GRAY, G. W., and GOODBY, J. W. G., 1984, *Smectic Liquid Crystals—Textures and Structures* (Leonard Hill).
[12] DOUCET, J., LEVELUT, A.-M., and LAMBERT, M., 1974, *Phys. Rev. Lett.*, **32,** 301.
[13] DE JEU, W. H., and DE POORTER, J. A., 1977, *Phys. Lett.* A, **61,** 114.
[14] DOUCET, J., and LEVELUT, A.-M., 1977, *J. Phys.*, **38,** 1163.
[15] GUILLON, D., and SKOULIOS, A., 1977, *J. Phys.*, **38,** 79.
[16] MCMILLAN, W. L., 1973, *Phys. Rev.* A, **8,** 1921.
[17] WULF, A., 1975, *Phys. Rev.* A, **11,** 365.